

Biophysical Journal, Volume 98

Supporting Material

Counter-intuitive stochastic behavior of simple gene circuits with negative feedback

Tatiana T. Marquez-Lago and Jörg Stelling

Supplementary Material

Counter-intuitive stochastic behavior of simple gene circuits with negative feedback

Tatiana T. Marquez-Lago^{1,2} and Jörg Stelling^{1,2}

¹ Department of Biosystems Science and Engineering and ² Swiss Institute of Bioinformatics, ETH Zurich, Mattenstrasse 26, 4058 Basel, Switzerland.

1. Biological ranges of parameters and sets fixed parameters considered in the simulations

	Description	Range	Units	Ref
α	Negative feedback parameter	$10^{-20} - 10^{15}$	M^{-1}	1, 2
k_1	TF (case 1-3) or mRNA (case 4-7) production rate	$10^{-3} - 2 \cdot 10^{-1}$	s^{-1}	1, 3
k_2	Rate of repressor binding to gene	$10^8 - 2 \cdot 10^{11}$	$M^{-1} s^{-1}$	2, 3
k_3	DNA-TF(2) dissociation rate	$\frac{k_2}{\alpha}$	s^{-1}	By definition
k_4	TF degradation rate	$2 \cdot 10^{-5} - 10^{-2}$	s^{-1}	1, 3
k_5	Rate of RNA polymerase binding to gene	$10^9 - 10^{11}$	$M^{-1} s^{-1}$	Calculated from 2
k_6	DNA-RNA polymerase dissociation rate	$1 - 10^3$	s^{-1}	4
k_7	mRNA degradation rate	$10^{-4} - 10^{-1}$	s^{-1}	1, 5
k_8	mRNA translation rate	$10^{-3} - 1$	s^{-1}	1, 5
k_9	TF dimerization rate	$5 \cdot 10^7 - 3 \cdot 10^8$	$M^{-1} s^{-1}$	6, 7, 8
k_{10}	TF dimer dissociation rate	$1 - 10^3$	s^{-1}	4

Table S1. Ranges of values to consider when tuning rates and reporting noise measurements.

	Description	Value	Units	Ref
k_1	TF / mRNA production rate	10/60	s^{-1}	
k_2	Rate of repressor binding to gene	10^8	$M^{-1} s^{-1}$	
k_4	TF degradation rate	10^{-4}	s^{-1}	1,3
k_5	Rate of RNA polymerase binding to gene	$1.8 \cdot 10^{10}$	$M^{-1} s^{-1}$	3
k_6	DNA-RNA polymerase dissociation rate	1	s^{-1}	
k_7	mRNA degradation rate	10^{-2}	s^{-1}	1,5
k_8	mRNA translation rate	10/60	s^{-1}	1,5
k_9	TF dimerization rate	$5 \cdot 10^7$	$M^{-1} s^{-1}$	
k_{10}	TF dimer dissociation rate	1	s^{-1}	
P	RNA polymerase	10^{-7}	M	

Table S2. Basic simulation parameter set 1. This set of parameters lies well inside biologically feasible ranges and portrays prototypical values found in the literature.

	Description	Value	Units	Ref
k_1	TF / mRNA production rate	10/60	s^{-1}	
k_2	Rate of repressor binding to gene	10^{10}	$M^{-1} s^{-1}$	
k_4	TF degradation rate	10^{-4}	s^{-1}	1,3
k_5	Rate of RNA polymerase binding to gene	$5 \cdot 10^9$	$M^{-1} s^{-1}$	Calculated from k_p in 3
k_6	DNA-RNA polymerase dissociation rate	10/60	s^{-1}	Calculated from k_p in 3
k_7	mRNA degradation rate	10^{-2}	s^{-1}	1,5
k_8	mRNA translation rate	1/60	s^{-1}	1,5
k_9	TF dimerization rate	10^9	$M^{-1} s^{-1}$	
k_{10}	TF dimer dissociation rate	1	s^{-1}	
P	RNA polymerase	10^{-7}	M	

Table S3. Simulation parameter set 2. This set of parameters was chosen to illustrate a middle point in the range of variation for k_2 . This value is significantly lower than the one used in (2) but potentially too large (6). Since the rate of dimerization of the repressor is thought to be approximately the same order as the binding of the repressor to the DNA, we fixed the value of k_9 to be 10^9 , which lies slightly outside the range found in the literature. We additionally chose rate k_6 to be slightly outside its range to be the same order as k_1 , in order to check whether a balance of the two rates reported significant deviation to the typical case when $k_1 < k_6$ is considered. Surprisingly, no noticeable difference was observed in terms of noise change or qualitative behavior as when using the equivalent rate values of parameter set 1.

2. Adopting the right modeling regime.

The very first step for accurately representing gene regulatory systems is building the right model within the right regime. Namely, one has to define a set of relevant chemical reactions and determine whether the biochemical phenomena are best described by stochastic or deterministic interactions, with temporal or spatio-temporal resolution, and embedded in a discrete or continuous regime, among other possibilities. A continuous deterministic approach, such as a differential equation model, is only adequate when dealing with large numbers of molecules and when discreteness and internal noise have no noticeable macroscopic effects. However, if the number of molecules of some species is small or if the system is susceptible to noise amplification, one has to inevitably consider a discrete stochastic approach. This applies, in particular, to gene regulatory systems with feedback control.

Fundamentally, the dynamics of chemical reaction networks are described by the chemical master equation (CME), and the PDF we are interested in is the solution to the CME. The CME describes the time evolution of the probability $P(X, t)$, for having $\mathbf{x} = [x_1, \dots, x_N]$ molecules in a system with R elementary reactions, N molecular species, and volume Ω at time t . With reasonable assumptions (16), one defines a set of propensity functions $\alpha_j(\mathbf{x})$ that measure the probability of each reaction happening. The propensities depend only on the current state \mathbf{x} . Hence, the process is memory-less and considered Markovian. It can be shown that for any state \mathbf{x} , the PDF satisfies the following discrete parabolic partial differential equation (PDE), subject to appropriate initial and boundary conditions:

$$\frac{\partial P(\mathbf{x}; t)}{\partial t} = \sum_{i=1}^R \alpha_i(\mathbf{x} - \mathbf{v}_i) P(\mathbf{x} - \mathbf{v}_i; t) - P(\mathbf{x}; t) \sum_{i=1}^R \alpha_i(\mathbf{x})$$

where $\mathbf{v}_j \in \mathbb{R}^n$ is the stoichiometric vector associated with reaction $j \in [1, R]$, defining the way the state \mathbf{x} transitions to state $\mathbf{x} + \mathbf{v}_j$ when reaction j occurs. The CME is then a set of such PDEs, where each equation corresponds to each possible state of the system.

Stochastic processes can be studied by trajectory based approaches or by their underlying probability distribution function (PDF), which tracks how the probability of having a certain number of molecules changes over time. A PDF approach is in many ways desirable, but computationally intensive if not impossible to attain, especially as the dimension of the model grows. This is one of the main reasons why Monte Carlo and trajectorial approaches have become so popular. Nevertheless, PDF approaches can sometimes – although rarely - be more computationally efficient than trajectory based approaches, so always sticking to a trajectorial approach should be taken with a pinch of salt.

3. Metrics for noise characterization

In general, there are two ways in which stochasticity can be considered. The 'single cell' type (Fig. S1a) or the 'multiple-cell' type (Fig. S1b). Preliminary stochastic simulations gave identical average results for both types of simulation, the reason why we decided to report our results under the first framework (Fig. S1a). It is not surprising that both frameworks yielded similar simulation results as intrinsic stochastic noise is inherently a Markovian process and by consequence, both cases can be considered mathematically equivalent. However, when it comes to experimental results that report noise measurements stemming from independent cells one should be a bit cautious since some factors, such as plasmid transfection or cell-cycle stage, cannot be considered homogeneous.

Here, we chose the CV for preliminary noise measurements based on independent exact trajectories of the CME for two reasons. First and foremost, the coefficient of variation is a more suitable basis for experimental interpretations (9). Secondly, we observed in preliminary numerical simulations of the 'RNAP' module that the Fano factor, defined as the variance of the observations divided by their mean, clearly contradicts noise behavior observations (data not shown). Moreover, the protein distribution in models with different underlying assumptions need not necessarily be Poissonian.

A last important note with respect to noise assessment is the source considered for the calculation of the CV. Unfortunately, there are several definitions of noise sources throughout the literature. Quite frequently one can find identical terms referring to different concepts, making it difficult to determine whether two analyses with seemingly contradictory results actually refer to the same issues. For example, in (9) the author portrays several ways in which noise sources can be classified, specifying that intrinsic noise is due to random births and deaths of individual molecules, and extrinsic noise due to fluctuations in reaction rates. The author explains that the terms 'intrinsic' and 'extrinsic' make a distinction between the origin and propagation of noise; their biological meaning being always defined with respect to a specified component or process. For example, in gene expression the total protein noise is divided into intrinsic (protein 'birth' and 'death' processes) and extrinsic (mRNA and gene terms). On the other hand, other studies such as (10) define all three sources as intrinsic to distinguish them from extrinsic fluctuations in the overall state of the cell. To complicate things further, some studies use the equivalent terms internal and external, the latter referring to e.g. particular states of the cell-cycle or environmental fluctuations, or even make distinctions between sources of extrinsic noise (11).

In our case, we calculate the CV of 'classic' internal noise, i.e. with respect to dynamic differences stemming from the stochastic decisions of when the next reaction occurs in the system, and what type of reaction it is. With respect to the terminology used in (9) it probably sums up to 'total protein noise',

although we find the term a bit uncomfortable given that some external factors can actually contribute to protein variations considerably, making the term 'total protein noise' insufficient.

4. Notes on lumped transcription-translation QSS models

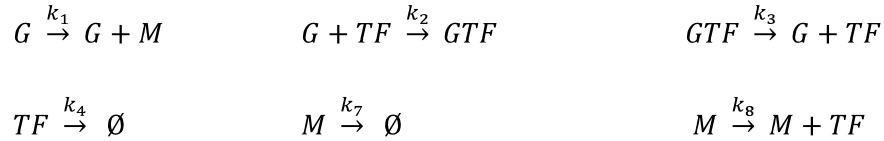
As mentioned in the main text, stochastic trajectories of the Chemical Master Equation do not necessarily resemble solutions of a perturbed ODE system, the reason why we decided to double-check the results in (3). In order to explore the potential differences in noise profiles, we obtained independent exact trajectories of the CME through the stochastic simulation algorithm (SSA) and compared our CV measurements with those obtained in (3).

Quite interestingly, when we fixed all reaction rate parameters and varied the feedback strength alone, the distributions of TF numbers of the unregulated and autoregulated systems were quite distinct. Notably, the unregulated case had a much smaller variation ($CV_{\text{unreg}} = 4 \cdot 10^{-6}$ and $CV_{\text{reg}} = 5 \cdot 10^{-4}$ for the unregulated and regulated case, respectively) (Fig. S2A). However, the steady state concentration of TF decreases with increasing feedback (Fig. S3) and one could argue the lower molecular numbers lead to increased noise with feedback. To eliminate this influence, we next fixed the steady state of TF to 1,000 molecules by tuning the protein production rate (k_1) accordingly (Fig. S2B,). In this case, the CVs of the unregulated and autoregulated systems were almost identical ($4.310 \cdot 10^{-4}$ and $4.6 \cdot 10^{-4}$). These results agree with previous findings (13) and are contrary to the original analysis (3), underlining the critical importance of noise metrics.

Similarly, when analyzing the 'RNAP' and 'DM' modules (as well as their combination), none of the systems displayed noise increase nor, counter intuitively, extreme noise attenuations with increasing gain of the negative feedback. The steepest noise attenuation was achieved when tuning the RNA polymerase binding/unbinding rates (k_5, k_6) followed by the TF degradation rate (k_4). Tuning rates that capture TF dimerization (k_9, k_{10}) even showed no noticeable noise variation with respect to increasing feedback. This underlines that detailed analyses of parameter spaces are required for characterizing noise behavior even of simple gene circuits. In Fig. S6A/D it can be observed that with identical model structure, feedback strength, and average TF levels, noise behavior depended on the specific parameterizations of the circuits, that is, the parameter used for tuning. These differences did not result from insufficient sampling of trajectories because the associated standard deviations were low (Fig. S6B,E).

5. Example: the ‘TT’ module. Parametrization assuming a QSS, the FSP and calculation of the moments of its CME

The ‘TT’ module consists of six elementary reactions. For this example we have four molecular species: gene (G), mRNA (M), transcription factor (TF) and gene bound with transcription factor (GTF); the sum of all states of the gene is always equal to one. Using the terminology from Fig. 1B (main text) the reactions (without preferential order) are:



If we further assume the reactions portraying repressor binding/unbinding to the gene to be much faster than all other reactions, a QSS in the states of the gene can be obtained. The first step is to derive the steady state of the ODEs for species G and GTF , later on introducing them in the ODEs for M and TF :

$$\begin{aligned}
 \frac{dM}{dt} &= \frac{k_1}{1 + \alpha TF} - k_7 M \\
 \frac{dTF}{dt} &= k_8 M - k_4 TF
 \end{aligned}$$

The parametrization of a particular system is obtained by factorizing a single rate from the steady state of the ODE system. Here, we have:

$$\begin{aligned}
 k_1 &= \frac{k_4 k_7 TF (k_3 + k_2 TF)}{k_3 k_8 (AV^{-1})} \\
 k_4 &= \frac{k_1 k_3 k_8 (AV^{-1})}{k_7 TF (k_3 + k_2 TF)} \\
 k_7 &= \frac{k_1 k_3 k_8 (AV^{-1})}{k_4 TF (k_3 + k_2 TF)} \\
 k_8 &= \frac{k_4 k_7 TF (k_3 + k_2 TF)}{k_1 k_3 (AV^{-1})}
 \end{aligned}$$

where AV is Avogadro’s number multiplied by the volume (in this case one femtoliter) and $\alpha = k_2/k_3$.

When tuning the parameter α we assume rate k_2 to be fixed.

In the ‘‘Stochastic discrete effects’’ section of the main text we mentioned that random changes at the mRNA level lead to a protein scaling behavior according to the difference between the reachable integer

numbers of mRNA molecules and the deterministic steady state solution for the mRNA. In order to illustrate this let us consider a deterministic quasi-steady state of the repressor $\widehat{TF} = 100$ in the 'TT' module, a prototypical scenario where jumps to states with higher TF numbers are visible. The corresponding state for \widehat{mRNA} will settle to 0.6 molecules ($\widehat{TF} = k_8 \widehat{M} / k_4 \sim 166 \widehat{M} = 100$).

With discrete molecule levels and high regulation, the mRNA level will either stick to the initial value –with high probability- or visit close-by states. With a ratio of $1/0.6 \sim 1.66$, a set of commonly visited states of the system naturally revolves around 166 molecules of TF.

In order to obtain the FSP of our system, we focused on the establishment of a 'dynamic equilibrium'. We use the term 'dynamic' in the sense that noise prevents the system from remaining at one state for long periods of time, and that the probability of reaching many states from a particular initial condition can vary considerably (14,15). In more detail, we explored the scenarios under which the mRNA level could be equal to 0, 1 and 2 molecules using the FSP (16) considering 1050 indexed possible states of the system. This corresponds to the states with TF varying between 1 and 350 molecules and mRNA varying between 0, 1 and 2 molecules, as these were bounds on reachable states observed in several stochastic trajectories with the initial state being $TF = 100$ and $mRNA = 1$. First, we obtained the probability for each state after 10^5 seconds, which is identical to the time span for the SSA simulations (Figs. S8 and S9) using two sets of nominal reaction rates. However, differences of the columns of the FSP higher than 10^{-2} indicated that the system was not close to a 'dynamic equilibrium', the reason why we further obtained the probability for each state after 10^9 seconds and compared with the corresponding SSA simulations. Interestingly, even when genetic regulation is a Markovian process and any reachable mRNA level is achievable at any time point, the span of probabilities of the reachable states is only revealed when considering the state matrix at 'dynamical equilibrium'.

Our simulations highlighted the dependency of numbers of mRNA molecules on both system's parameters and feedback level. Moreover, the FSP shows 'islands' of high probability around the 'increased' TF states that are a result of the augmented mRNA concentration (Supplementary Fig. S10). Both results fit well with corresponding SSA simulation results (Supplementary Tables S2 and S3, Fig. S8 and S9) and suggest the dependency on the exact parameter configuration, even with fixed feedback and steady-state initial TF levels.

There are a few algorithmic subtleties to note. We believe our choice of analyzed system's states highlights typical prokaryotic gene expression scenarios, for which the FSP algorithm ran quite efficiently. However, if the inclusion of other possible states deems to be relevant, a Krylov-based FSP such as (15) would be preferable.

In the “Protein bursts” section of the main text we mentioned that tuning rates k_4 and k_8 alongside feedback strength can result in random but sudden bursts of protein production. Given the observed size of the protein bursts, an extremely large number of possible system states has to be considered. Hence, computing the PDF through the FSP is not an option. Nevertheless, for calculating the moments of the CME, one can follow the methodology of (1, their Supplementary Material), where exact solutions for the moments of linear systems are found through:

$$\frac{d\langle f(x) \rangle}{dt} = \left\langle \sum_{\text{events}} \text{rate of event} \cdot \text{change of } f(x) \text{ due to event} \right\rangle$$

In (1), the authors obtain linearizations depending on feedback strength, and from there obtain expressions for the first and second moments (i.e. mean and variance). Using our notation, we can observe the CV

$$\frac{\sigma^2(\widehat{TF})}{\widehat{TF}^2} \sim \frac{1}{\widehat{TF}} \left(1 + \frac{k_8 - k_7}{2(k_4 + k_7)} \right)$$

Note that, since $k_8 = \frac{k_7 k_4 \widehat{TF} (1 + \alpha \widehat{TF})}{k_1}$, the tuned repressor translation rate increases with increasing feedback. Also, protein half-lives are longer than mRNA half-lives, which implies $k_4 < k_7$. With these two considerations one can see that:

$$\frac{\sigma^2(\widehat{TF})}{\widehat{TF}^2} \sim \frac{1}{\widehat{TF}} \left(\frac{k_1 (2k_4 + k_7) + k_4 k_7 \widehat{TF} (1 + \alpha \widehat{TF})}{2(k_4 + k_7)} \right) > \frac{1}{\widehat{TF}} \left(\frac{k_7 \widehat{TF} (1 + \alpha \widehat{TF})}{4k_1} \right) > \widehat{TF}$$

where the feedback parameter was transformed to numbers of molecules, to be consistent with units of other parameters. As was discussed in the main text, the CV largely disregards asymmetries in distributions. Nevertheless, due to the lack of any type of multimodality in this case, it can still hint at the average growth pattern of TF at high feedback levels.

6. Eigenvalues of associated deterministic systems

Here we present the case-by-case formula for the eigenvalue(s) of the associated deterministic systems. It should be noted that, within these formulas, TF is expressed in terms of molarity. Also, we use the shorthand notation:

$$k_p = \frac{k_5}{k_1 + k_6} , \quad \beta = \frac{k_9}{k_{10}}$$

Case 1 – 'RNAP' module

$$eig = - \frac{k_1 * k_p * P * \alpha}{(1 + \alpha * TF + k_p * P)^2 * V * Av} - k_4 \leq 0 \quad \forall \quad TF \geq 0$$

Case 2 - 'DM' module

$$eig = - \frac{2 * k_1 * \alpha * TF * \beta}{(1 + \alpha * \beta * TF^2)^2 * V * Av} - k_4 \leq 0 \quad \forall \quad TF \geq 0$$

Case 3 - 'RNAP' along with 'DM' modules

$$eig = - \frac{2 * k_1 * k_p * P * \alpha * \beta * TF}{(1 + \alpha * \beta * TF^2 + k_p * P)^2 * V * Av} - k_4 \leq 0 \quad \forall \quad TF \geq 0$$

Case 4 – 'TT' module

$$eig = \frac{1}{2 * (1 + \alpha * TF)} \left[-(k_4 + k_7) * (1 + \alpha * TF) \pm \sqrt{[(k_4 - k_7) * (1 + \alpha * TF)]^2 - \frac{4 * \alpha * k_1 * k_8}{V * Av}} \right]$$

$$if \quad [(k_4 - k_7) * (1 + \alpha * TF)]^2 < \frac{4 * \alpha * k_1 * k_8}{V * Av} \Rightarrow eig \in \mathbb{C}$$

Case 5 – 'RNAP' along with 'TT' modules

$$eig = \frac{1}{2 * (1 + \alpha * TF + k_p * P)} \left[-(k_4 + k_7) * (1 + \alpha * TF + k_p * P) \right. \\ \left. \pm \sqrt{[(k_4 - k_7) * (1 + \alpha * TF + k_p * P)]^2 - \frac{4 * \alpha * k_1 * k_8 * k_p * P}{V * Av}} \right]$$

$$if \quad [(k_4 - k_7) * (1 + \alpha * TF + k_p * P)]^2 < \frac{4 * \alpha * k_1 * k_8 * k_p * P}{V * Av} \Rightarrow eig \in \mathbb{C}$$

Case 6 - 'DM' along with 'TT' modules

$$eig = \frac{1}{2 * (1 + \alpha * \beta * TF^2)} \left[-(k_4 + k_7) * (1 + \alpha * \beta * TF^2) \right. \\ \left. \pm \sqrt{[(k_4 - k_7) * (1 + \alpha * \beta * TF^2)]^2 - \frac{8 * \alpha * \beta * k_1 * k_8 * TF}{V * Av}} \right]$$

$$if \quad [(k_4 - k_7) * (1 + \alpha * \beta * TF^2)]^2 < \frac{8 * \alpha * \beta * k_1 * k_8 * TF}{V * Av} \Rightarrow eig \in \mathbb{C}$$

Case 7 - 'RNAP' along with 'DM' and 'TT' modules

$$eig = \frac{1}{2 * (1 + \alpha * \beta * TF^2 + k_p * P)} \left[-(k_4 + k_7) * (1 + \alpha * \beta * TF^2 + k_p * P) \right. \\ \left. \pm \sqrt{[(k_4 - k_7) * (1 + \alpha * \beta * TF^2 + k_p * P)]^2 - \frac{8 * \alpha * \beta * k_1 * k_8 * TF * k_p * P}{V * Av}} \right]$$

$$if \quad [(k_4 - k_7) * (1 + \alpha * \beta * TF^2 + k_p * P)]^2 < \frac{8 * \alpha * \beta * k_1 * k_8 * TF * k_p * P}{V * Av} \Rightarrow eig \in \mathbb{C}$$

Interestingly, when tuning rates k_7 and k_8 , trajectories with protein bursts are only visible in areas where the overall noise growth is higher than that of the protein burst average jump $b = k_8/k_7$. To verify this, we computed the values R of the slopes of the logarithm of the noise divided by the values of the slopes of the logarithm of b , and checked the feedback values in which such ratio was larger or equal to 1. Tuning the mRNA transcription rate (k_8) always displayed protein bursts, i.e. for all considered steady

states of TF there were zones in which $R \geq 1$. On the other hand, tuning the mRNA degradation rate (k_7) yielded protein bursts for steady states of TF = 10 or lower, where $R \geq 1$ as was already expected. However, for steady states of $TF \geq 100$ we observed that $R < 1$ and stochastic focusing was the driving force behind noise increase. Illustrative examples can be found in Figure S11 and S12.

However, having $R \geq 1$ cannot be considered a blind rule of thumb as it, by itself, cannot explain the increase of noise when tuning rates k_1 and k_4 with TF = 1 molecule. Quite contrary to what was observed in all cases that did not include mRNA transcription, we observed protein bursts scenarios while the value of b is invariant ($b = 1.6\bar{6}$).

Supplementary Figures

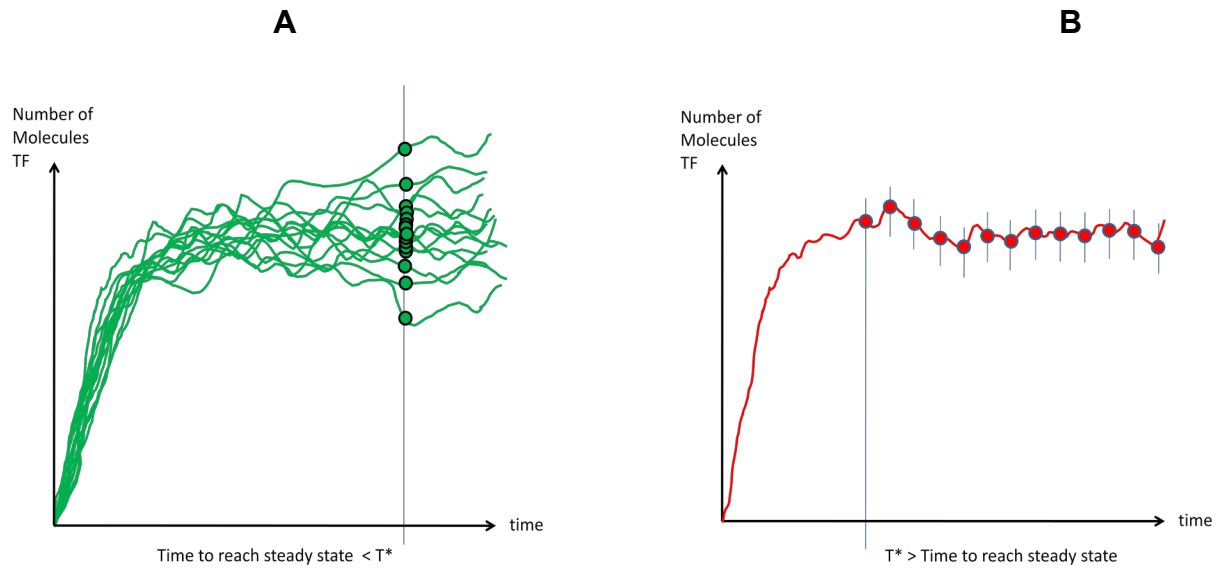


Figure S1. Two different types of collecting sample points of stochastic simulations. (A) Independent runs (corresponding to different cells) where for each simulation the number of molecules of TF is collected at the same time, T^* . (B) Single run (single cell experiment) where the number of molecules of TF is collected at equally spaced time steps, all of which lie beyond T^* . T^* is assumed to be a point in time beyond the average time it takes for a system to reach its steady state.

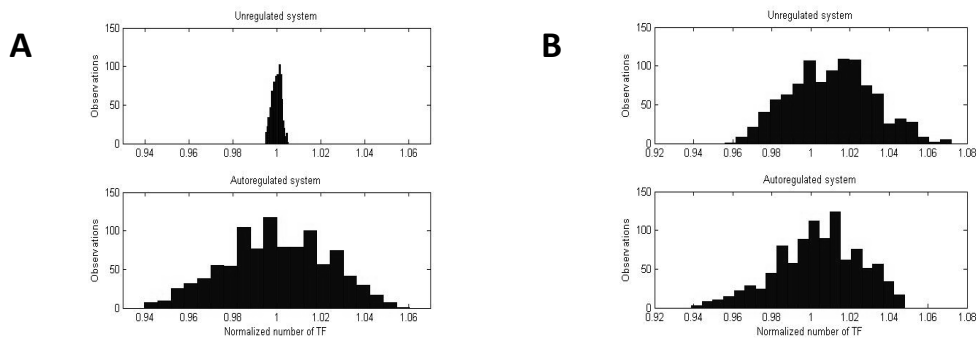


Figure S2. Histograms of normalized numbers of TF for the Becskei-Serrano model (6) using identical kinetic rate constants. Stochastic simulation results were obtained (A) by fixing rate k_1 and increasing feedback from 0 to 2^{11} , and (B) by fixing the steady-state TF to 1,000 molecules and tuning k_1 accordingly. The values of 'unit one' correspond to normalized observations of the CV.

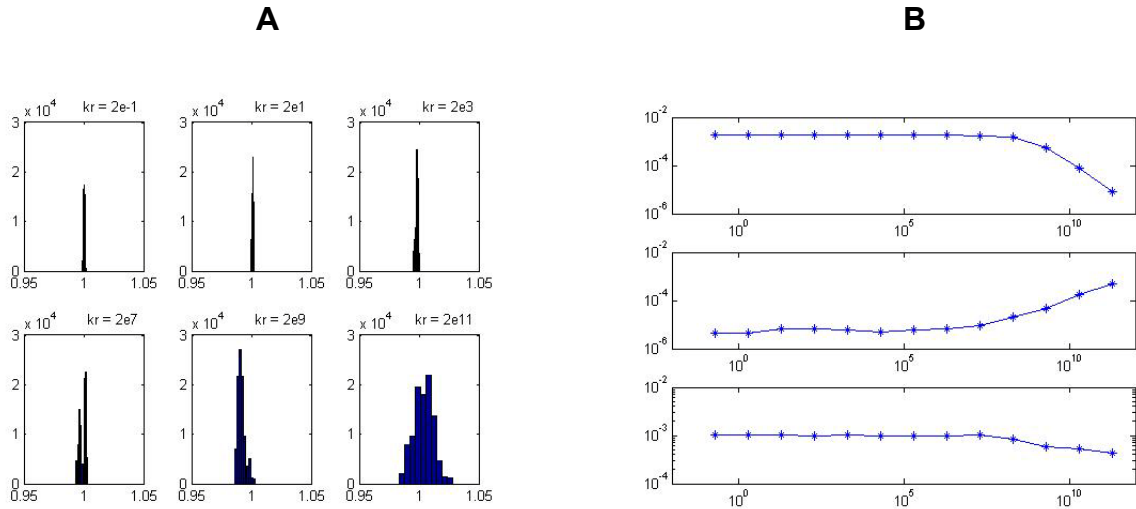


Figure S3. Discrepancies in noise measurements for the Becskei-Serrano model (3), where the feedback parameter is denoted by k_r , out of consistency with their notation. (A) Histograms of normalized number of molecules with increasing feedback strength. Molecule numbers were obtained at each second for a total of 10^4 seconds, normalizing to the steady state corresponding to each set of parameters (B) Number of molecules present in steady state (top), CV for each corresponding steady state and set of parameters (middle), CV for increasing feedback, while fixing the steady state by tuning k_r (bottom).

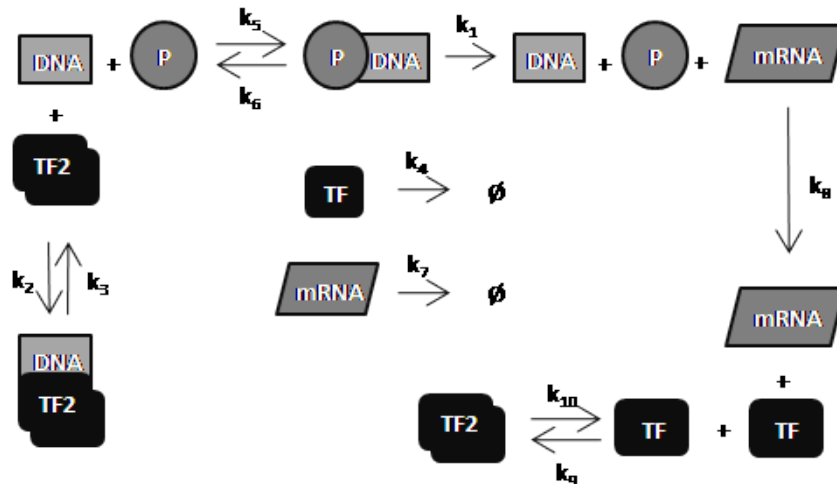


Figure S4. Combination of the three basic modules outlined in Fig. 1 of the main text.

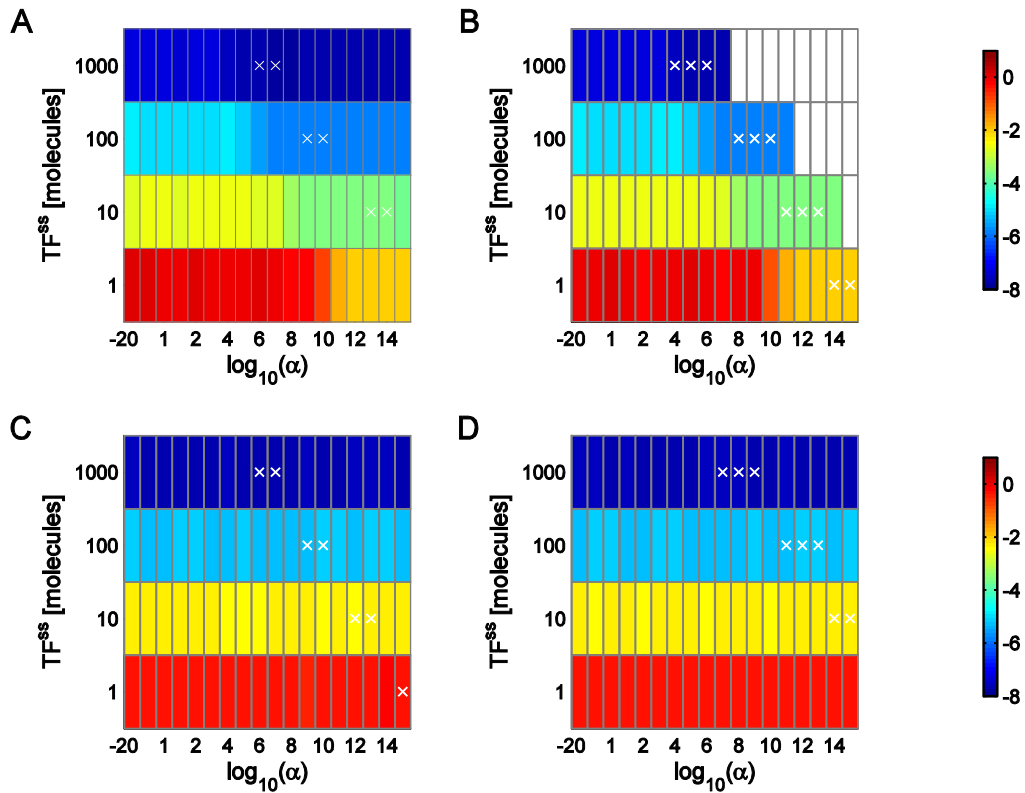


Figure S5. Average CV behavior for the models containing the 'RNAP' and 'DM' modules. CV behavior (color coded) is compared as a function of number of repressor proteins in deterministic steady state (used as initial condition) and of feedback strength. Colors show $\log_{10}(CV)$, white crosses indicate cases where all kinetic parameters are biologically feasible and empty boxes correspond to feedback values for which the reaction rate would be negative. Panels represent the CV when (A) tuning rate k_5 , the rate at which RNA polymerase binds to the gene, (B) tuning rate k_6 , DNA-RNA polymerase complex dissociation rate (C) tuning rate k_9 , the protein dimerization rate, (D) tuning rate k_{10} , the repressor homodimer dissociation rate.

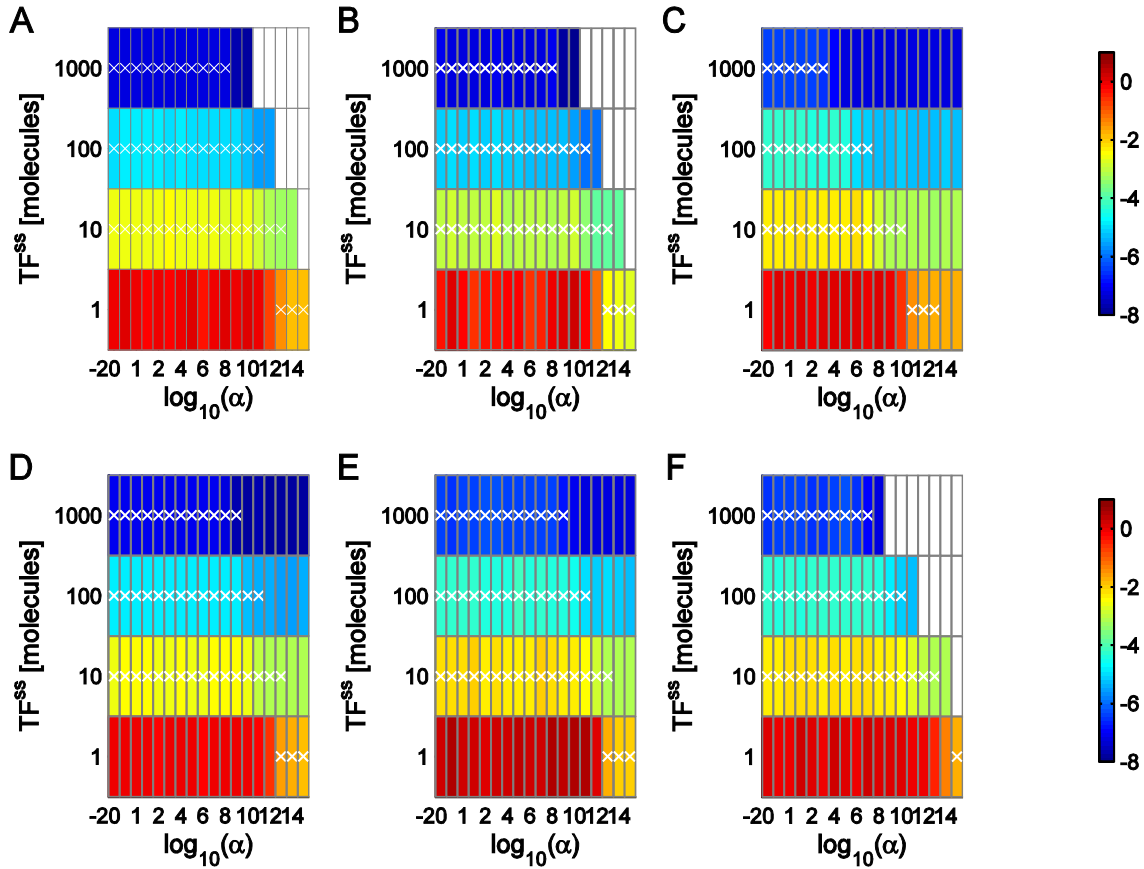


Figure S6. Noise behavior for models that lump transcription and translation in one step. CV (color coded) is compared as a function of TF in deterministic steady state (used as initial condition) and of feedback strength. Colors show $\log_{10}(\text{CV})$, white crosses indicate biologically feasible kinetic parameters, and empty boxes correspond to cases where the tuned rate is negative (hence unrealistic). (A,C,D,F) Average and (B,E) standard deviation of the CV. Cases correspond to (A,B,D,E) 'RNAP' module (C) 'DM' module and (F) 'RNAP' and 'DM' modules. (A-C,F) correspond to cases where rate k_1 , the rate at which the TF is produced, is tuned. (D,E) correspond to cases where rate k_4 , the TF degradation rate, is tuned.

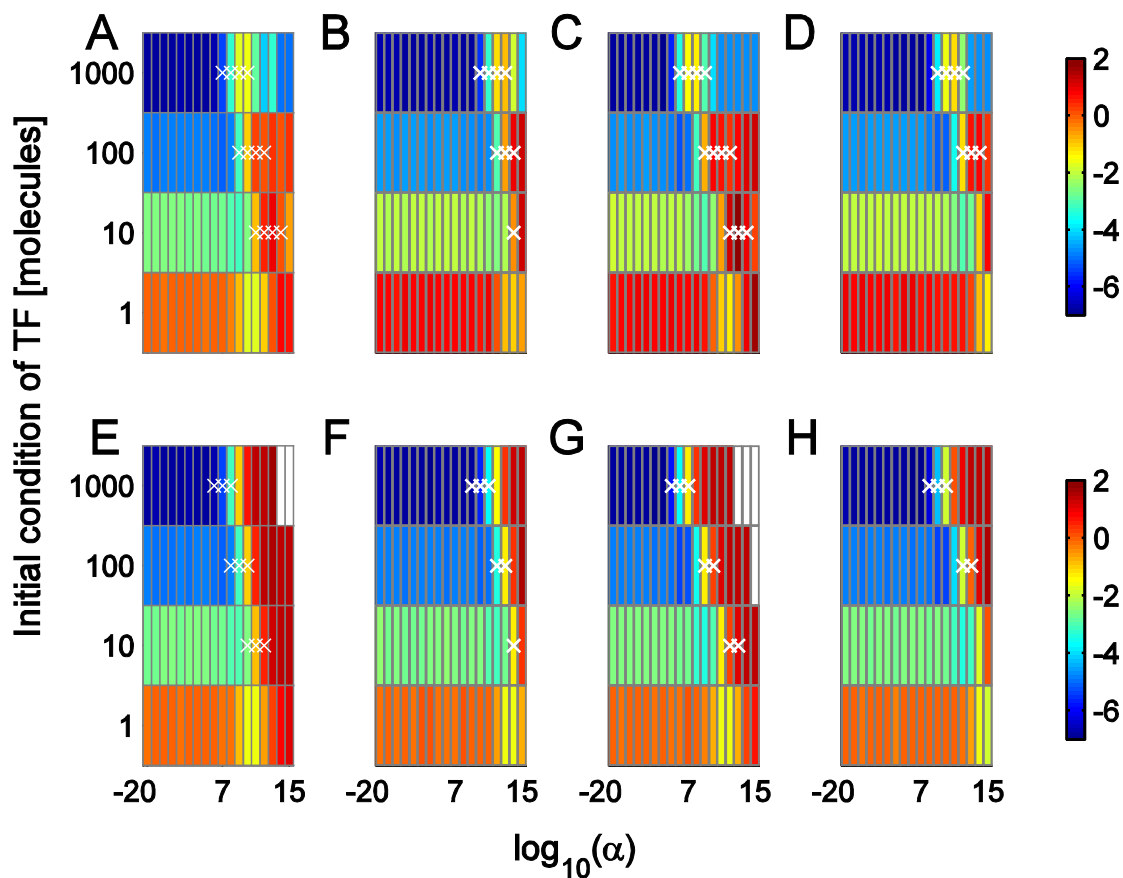


Figure S7. Feedback-dependent noise (CV) behavior of models that consider transcription and translation as separate processes. Steady state protein levels were fixed by tuning the mRNA degradation rate (k_7 , A-D) and the protein translation rate (k_8 , E-H), respectively. Columns refer to different models, namely (A,E) 'TT' module, (B,F) 'TT' and 'RNAP' modules, (C,G) 'TT' and 'DM' module, and (D,H) combination of all three modules. Colors show $\log_{10}(\text{CV})$ and white crosses indicate cases where all kinetic parameters are biologically feasible.

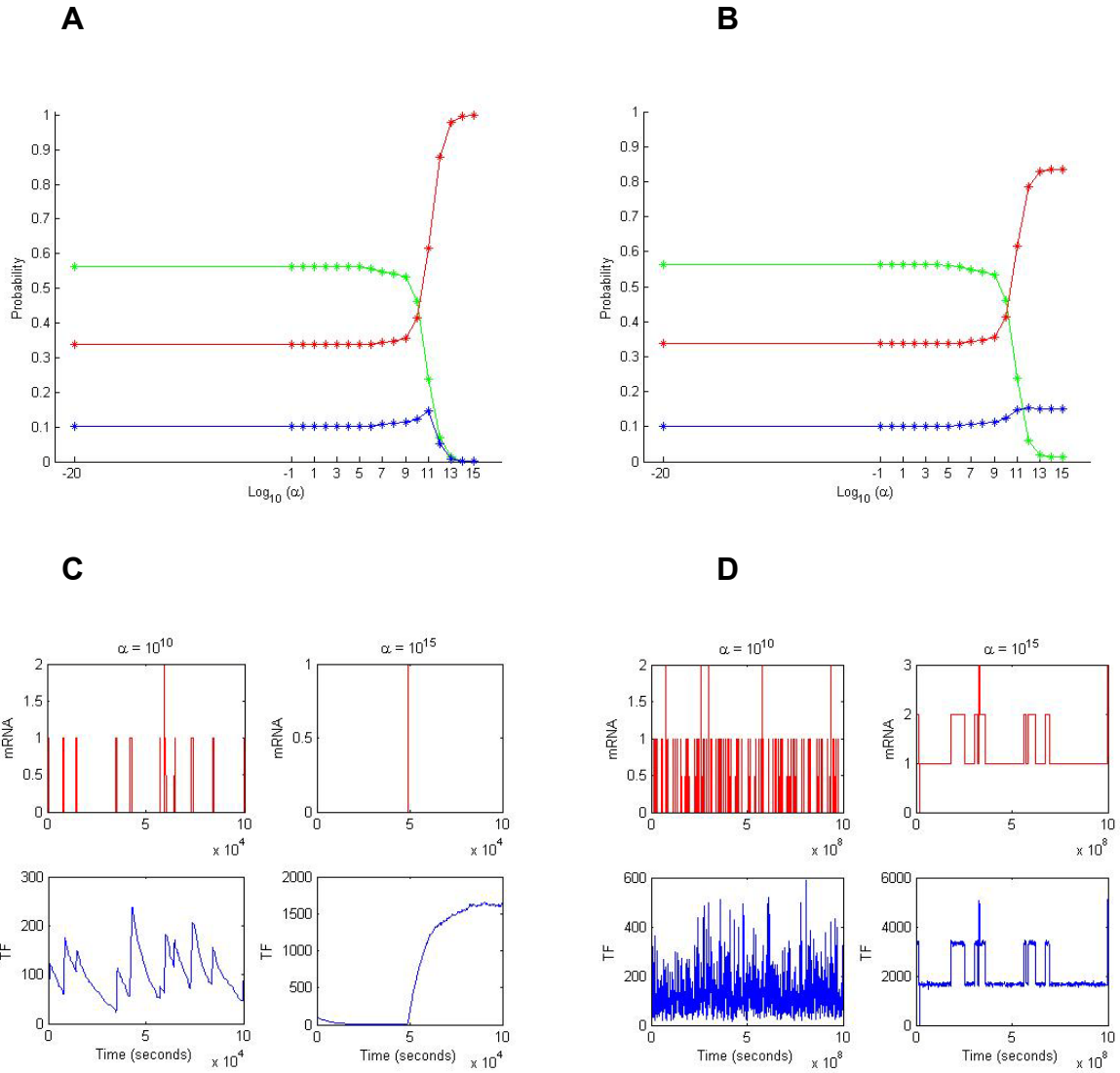


Figure S8. FSP of the 'TT' module, considering reaction rate set 2. The lines in green, red and blue refer to the probability of having 0, 1 and 2 molecules of mRNA, respectively. (A-B) FSP for all feedback values (A) evaluated at 10^5 seconds and (B) evaluated at 10^{15} seconds. (C-D) Corresponding SSA runs showing in red the mRNA level and in blue the number of molecules of TF, (C) total simulation time of 10^5 seconds with characteristic values of $\alpha = 10^{12}$ and $\alpha = 10^{15}$ (D) total simulation time of 10^9 seconds with characteristic values of $\alpha = 10^{10}$ and $\alpha = 10^{15}$.

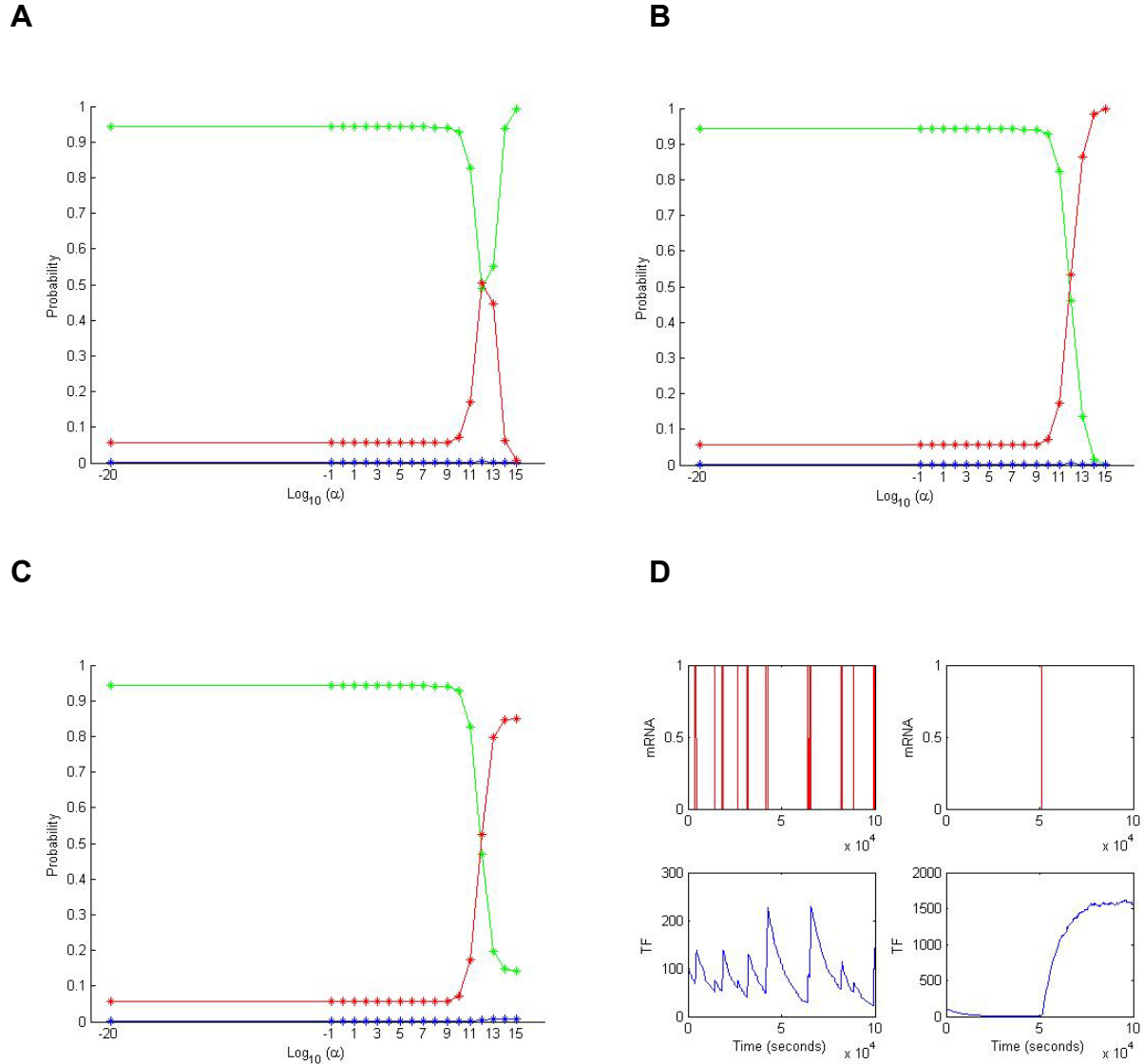


Figure S9. FSP of the 'TT' module, considering reaction rate set 1. The lines in green, red and blue refer to the probability of having 0, 1 and 2 molecules of mRNA, respectively. (A-C) FSP for all feedback values (A-B) evaluated at 10^5 seconds and (C) evaluated at 10^{10} seconds. The initial conditions used are a probability equal to one of being at state (A) $M = 0$, $TF = 100$, (B) $M = 1$, $TF = 100$ and (C) either case (identical probability profiles), (D) Corresponding SSA runs with characteristic values of $\alpha = 10^{10}$ and $\alpha = 10^{15}$ showing in red the mRNA level and in blue the number of molecules of TF, with a total simulation time of 10^5 seconds. From (A-B) it can be noticed that initial conditions have a great impact in the probability profiles when the FSP is not at 'dynamical equilibrium'. In (C) The probability of observing 2 mRNA molecules is minimal, but it should be noticed that the number of molecules of mRNA can in principle be higher. This is to be expected as the FSP did a truncation on the state space, and the probability of the states summed to almost one, the small remainder leaving room for cases with higher numbers of mRNA/TF molecules.

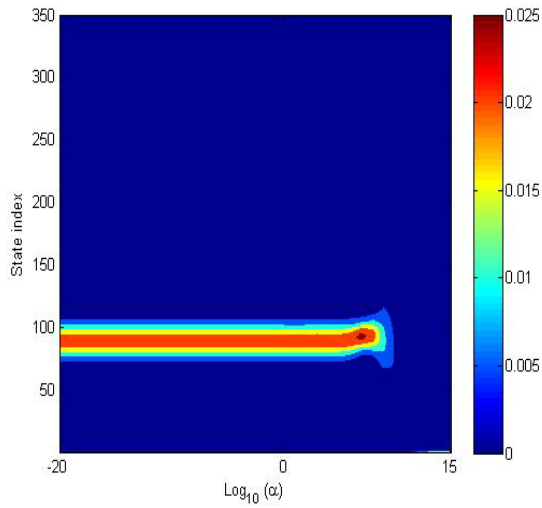
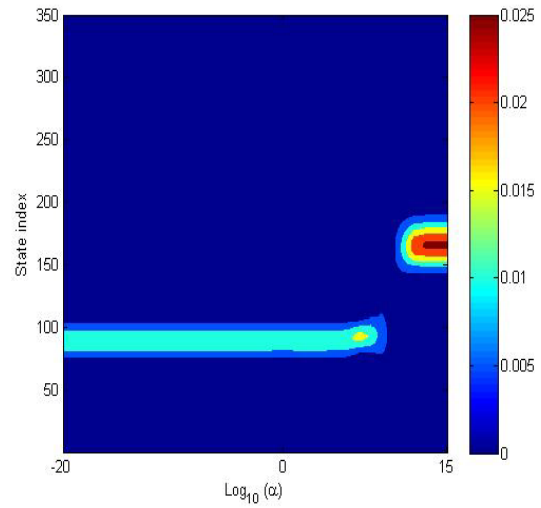
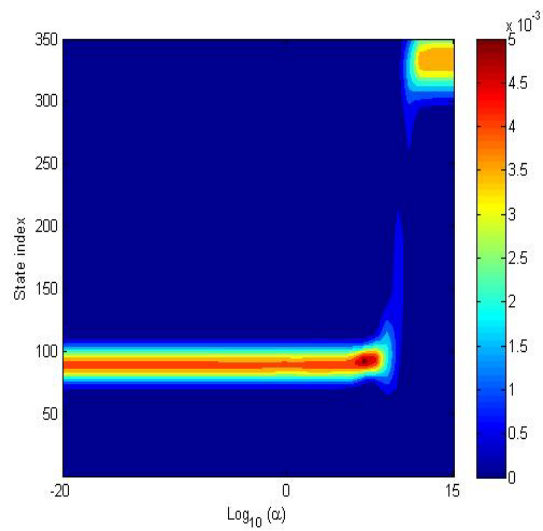
A**B****C**

Figure S10. Contour plots of the FSP algorithm applied to the 'TT' module, using the parameter set 2 while varying the mRNA degradation rate k_7 . Probability is studied case by case (i.e. depending on TF) (A) for having in the system 0 molecules of mRNA (B) 1 molecule of mRNA (C) 2 molecules of mRNA. Notice that the sum of the values in the contour 'columns' yields the probability for a particular feedback value to portray the corresponding number of molecules of mRNA.

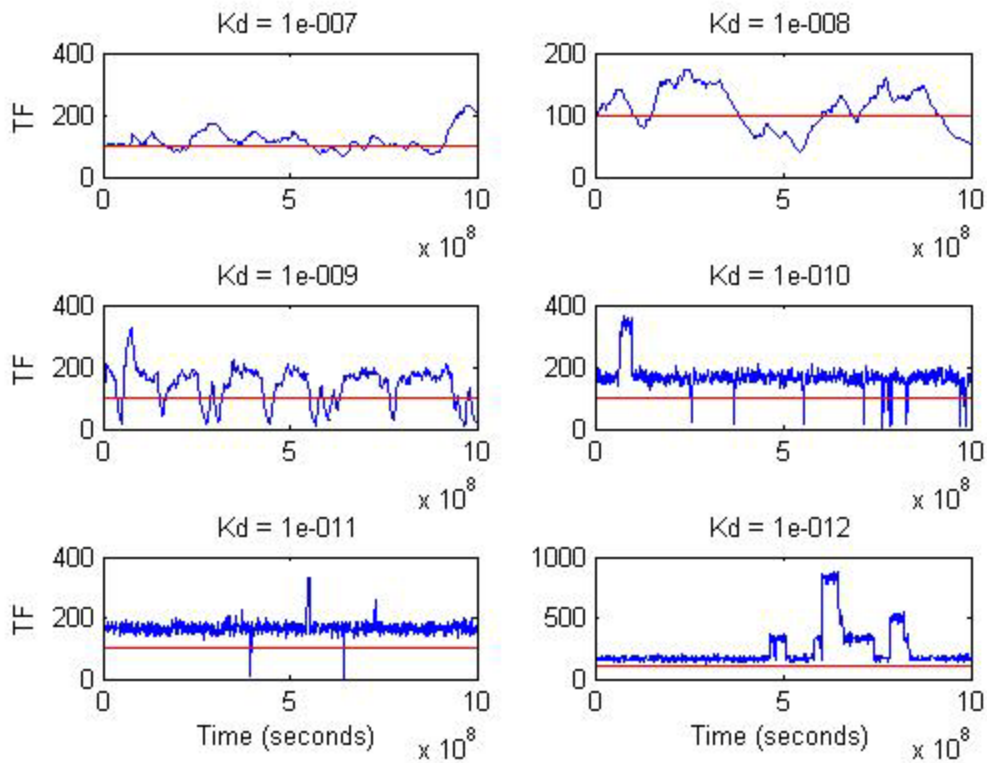


Figure S11. Time evolution of a sample stochastic focusing scenario, depending on different negative feedback strengths ($K_d = 1/\alpha$). Stochastic simulation of the 'TT' module (in blue) with an initial condition from the deterministic steady state of $TF = 100$ molecules (in red), using parameter set 2. The time span is larger than regular simulations, for illustration purposes.

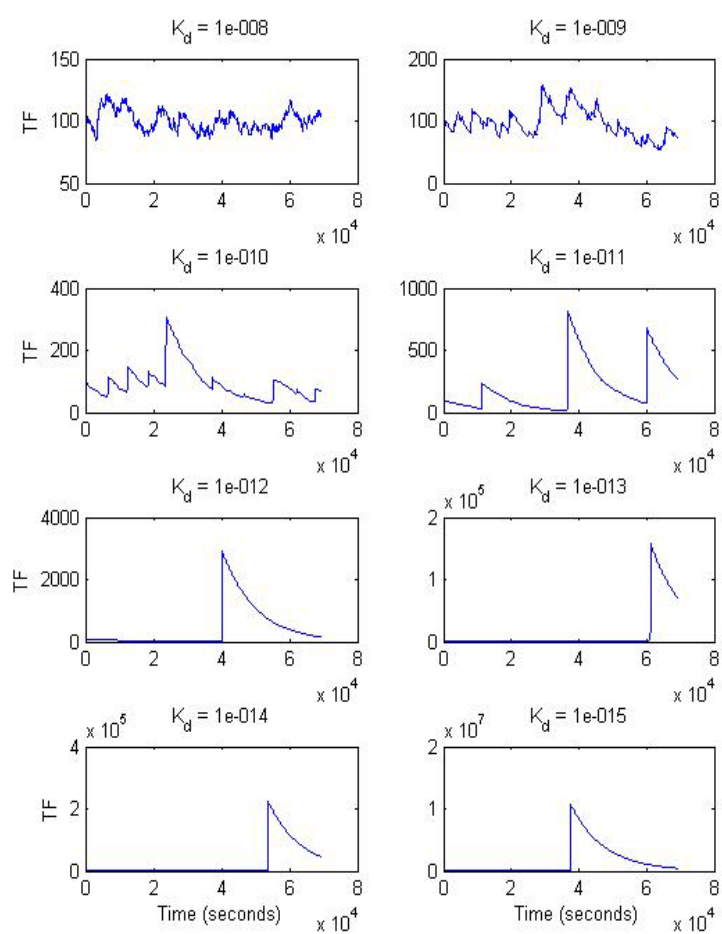


Figure S12. Time evolution of a sample protein burst scenario, depending on different negative feedback strengths ($K_d = 1/\alpha$). This simulation was obtained from simulating the ‘TT’ module (in blue) with an initial condition from the deterministic steady state of TF = 100 molecules (in red), using parameter set 2. Time span is larger than regular simulations, for illustration purposes.

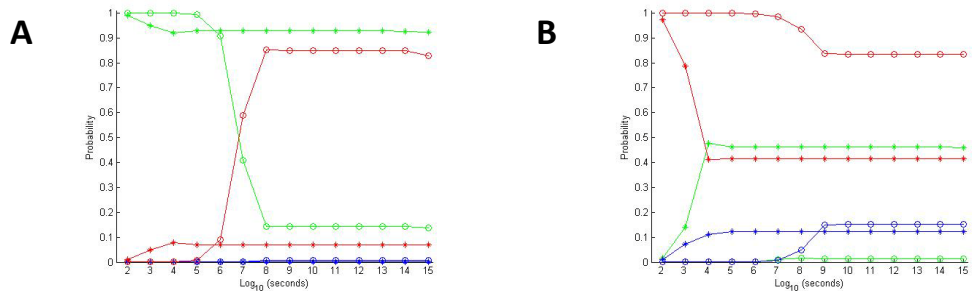


Figure S13. FSP of the 'TT' module, considering reaction rate set 1 (A) and set 2 (B), with fixed feedback $\alpha = 10^{10}$ (stars) and $\alpha = 10^{15}$ (circles). Probabilities are evaluated for times between 10^2 and 10^{15} seconds, time represented in log scale. The lines in green, red and blue refer to the probability of having 0, 1 and 2 molecules of mRNA, respectively.

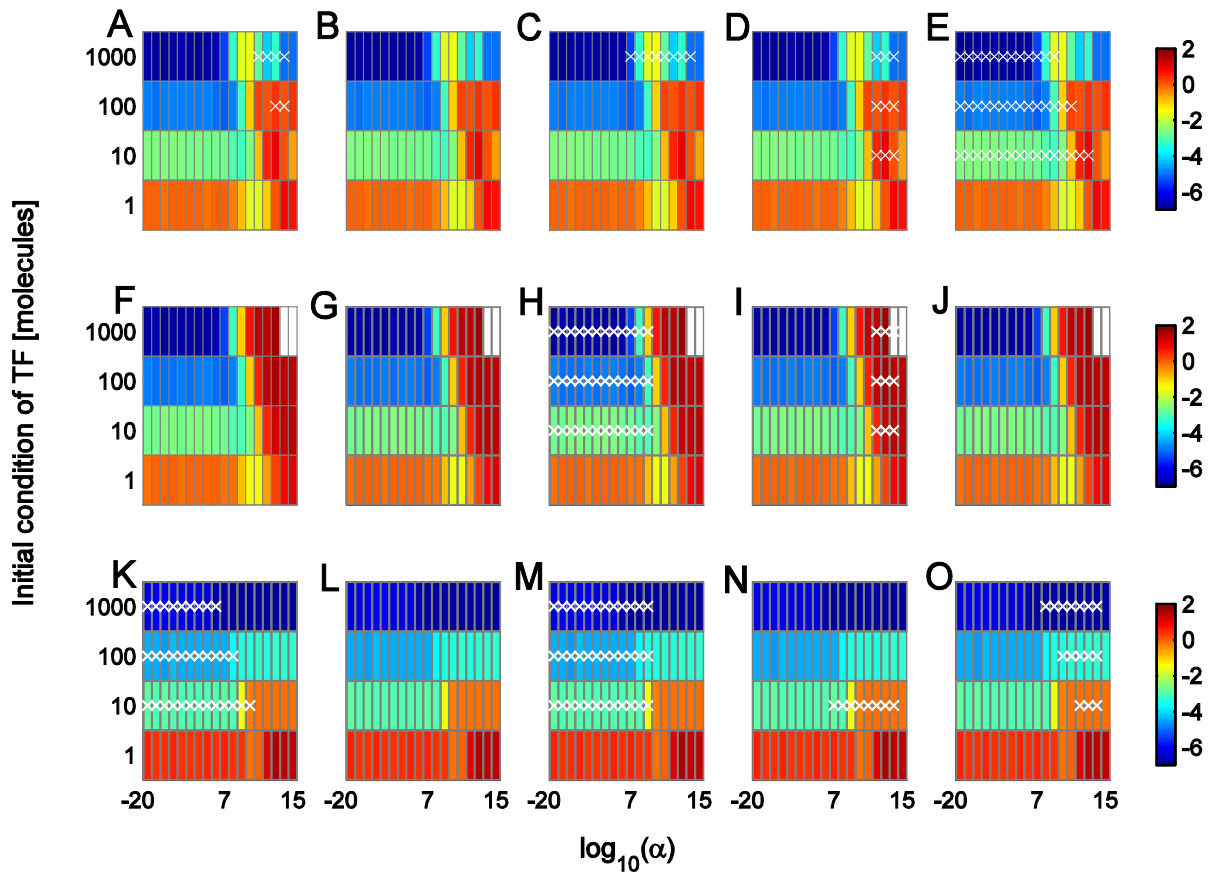


Figure S14. Feedback-dependent noise (CV) behavior of the ‘TT’ module while assuming a QSS, as compared with previously published criteria for burst-like behavior and multimodality. Steady state protein levels were fixed by tuning the mRNA degradation rate (k_7 , A-E), the protein translation rate (k_8 , F-J), and the protein degradation rate (k_9 , K-O), respectively. Columns refer to different test criteria, namely (A,F,K) if $k_4 > k_7$ the TF distribution will follow that of mRNA (B,G,L) if $k_4 > k_7$ the TF distribution will also follow that of mRNA (C,H,M) $k_2, k_3 < k_7$ yields bimodality (D,I,N) $k_2, k_3 < k_7$ yields bimodality and (E,J,O) if $k_3 < k_4$ yields bimodality and (E,J,O) if $k_7 \gg k_4$, -quantified here as an order of magnitude difference- one can observe protein bursts. Colors show $\log_{10}(\text{CV})$ and white crosses indicate cases predicted by the corresponding criterion.

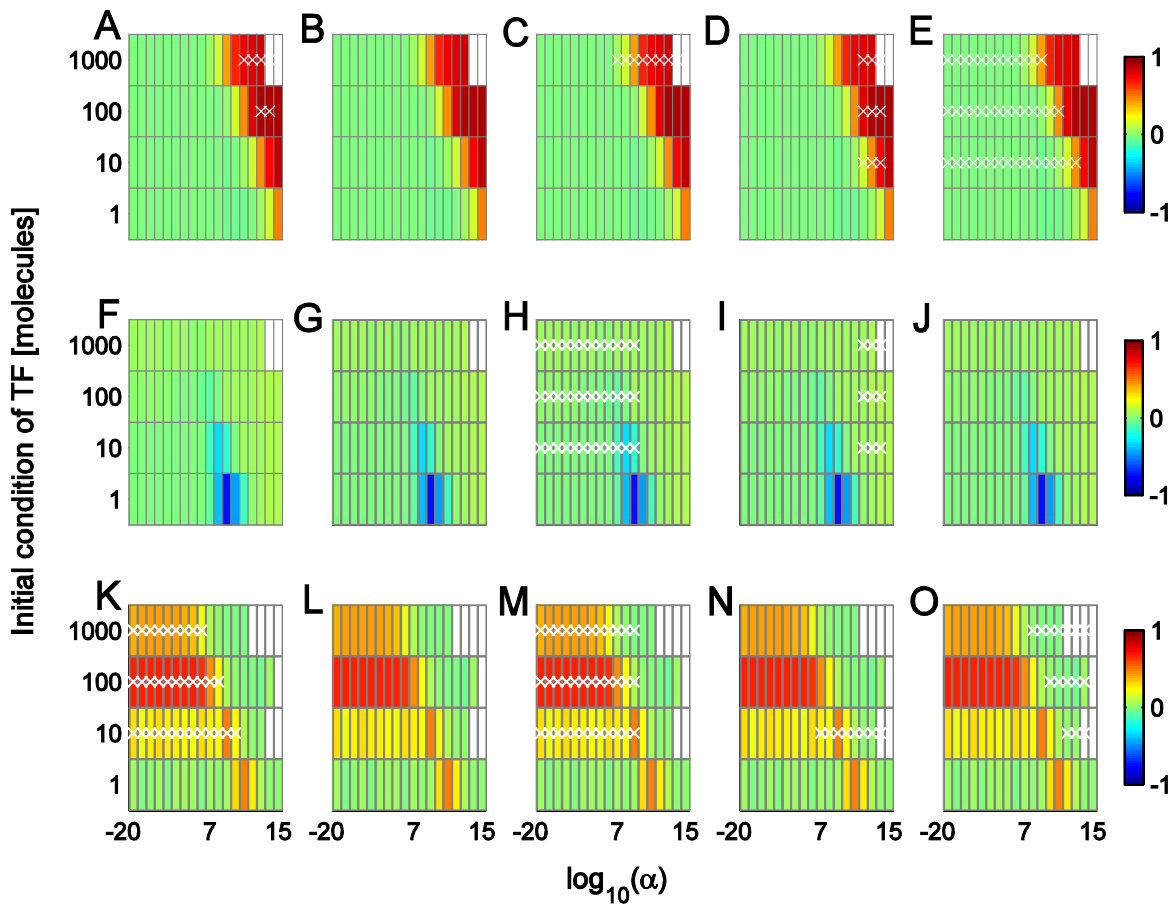


Figure S15. Time-correlation behavior of the ‘TT’ module while assuming a QSS, as compared with previously published criteria for burst-like behavior and multimodality. Steady state protein levels were fixed by tuning the mRNA degradation rate (k_7 , A-E), the protein translation rate (k_8 , F-J), and the protein degradation rate (k_8 , K-O), respectively. Columns refer to different test criteria, namely (A,F,K) if $k_4 > k_7$ the TF distribution will follow that of mRNA (B,G,L) if $k_2+k_3 < k_7 < k_4$ the TF distribution will also follow that of mRNA (C,H,M) $k_2, k_3 < k_7$ yields bimodality (D,I,N) $k_3 < k_4$ yields bimodality and (E,J,O) if $k_7 \gg k_4$, quantified here as an order of magnitude difference, one can observe protein bursts. Colors show $\log_{10}(\text{CV})$ and white crosses indicate cases predicted by the corresponding criterion. Empty boxes indicate relaxation to inactive gene state, or non-computable cases.

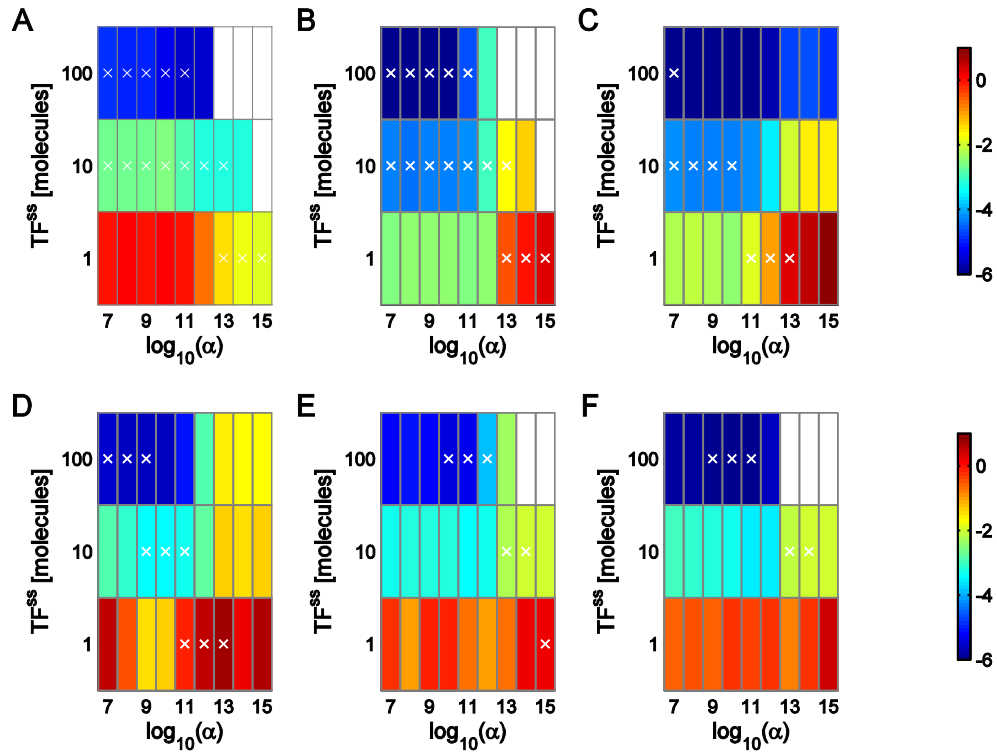


Figure S16. Comparison of average CV behavior for models with (A) and without a quasi-steady state assumption (B-F), while tuning rate k_1 (transcription or lumped transcription-translation rate). The CV behavior of 100 simulations (color coded) is compared as a function of number of repressor proteins in deterministic steady state (used as initial condition) and of feedback strength. Colors show $\log_{10}(\text{CV})$, white crosses indicate cases where all kinetic parameters are biologically feasible and empty boxes correspond to feedback values for which the reaction rate would be negative. Panels represent the CV when considering (A-B) the ‘RNAP’ module (C) the ‘DM’ module (D) ‘TT’ module (E) ‘TT’ along with ‘RNAP’ modules (F) ‘TT’ along with ‘DM’ modules.

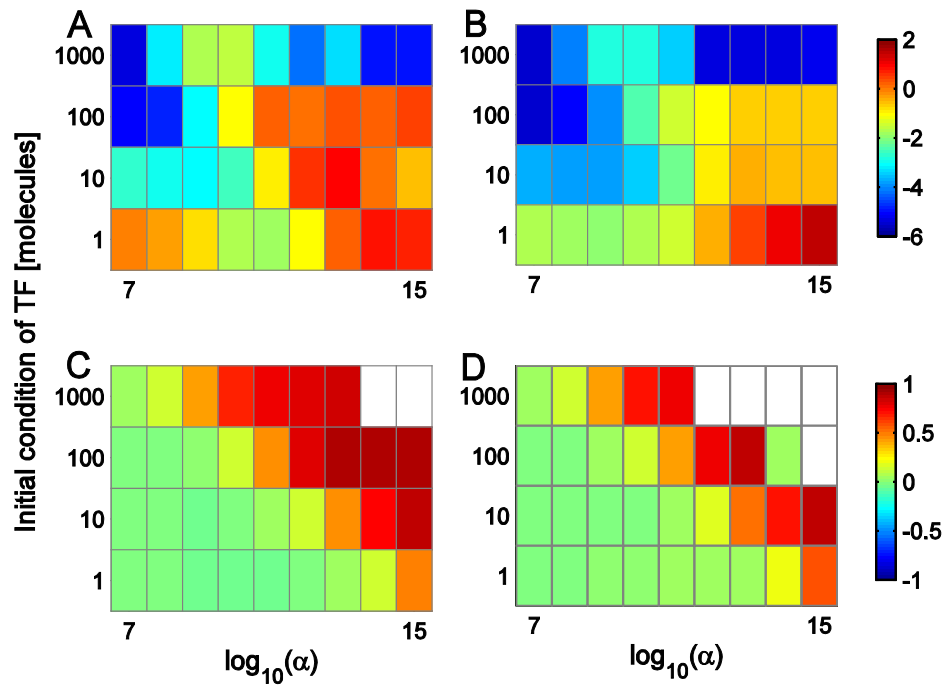


Figure S17. Comparison of the 'TT' module (A,C) with a QSS assumption and (B,D) without. Colors show $\log_{10}(CV)$ and steady state protein levels were fixed by tuning the mRNA degradation rate (k_7 , A-B) and the protein translation rate (k_8 , C-D).

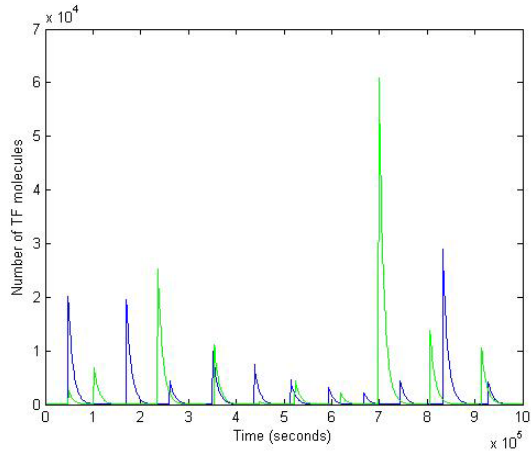
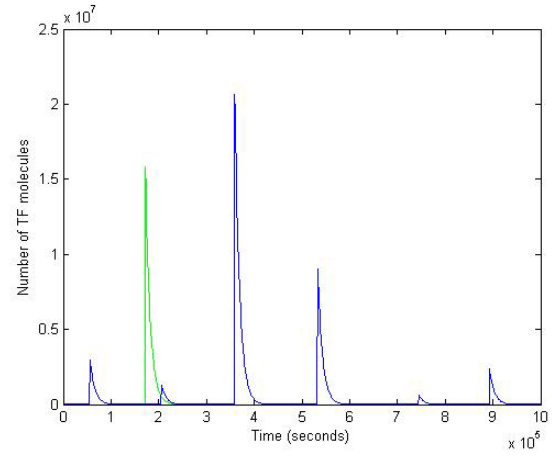
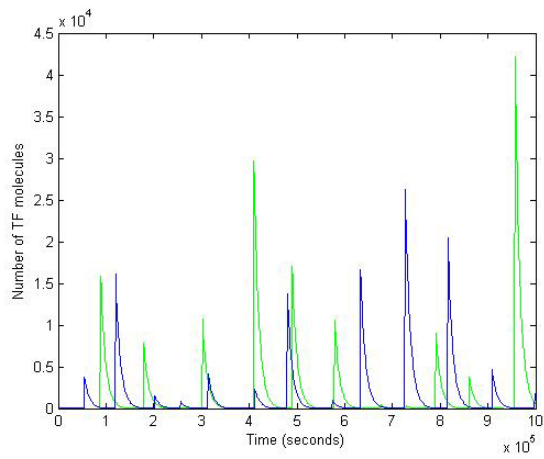
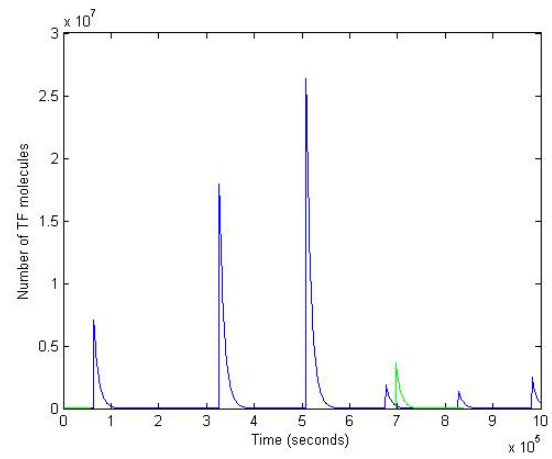
A**B****C****D**

Figure S18. Prototypical simulations of the 'TT' module with a QSS assumption (blue) and without (green). Protein bursts were obtained while varying the protein translation rate k_8 in a time scale of 10^6 seconds with (A-B) nominal reaction rate set 2 and (C-D) nominal reaction rate set 1. Figures correspond to cases where (A,C) $\alpha = 10^{12}$, (B,D) $\alpha = 10^{15}$.

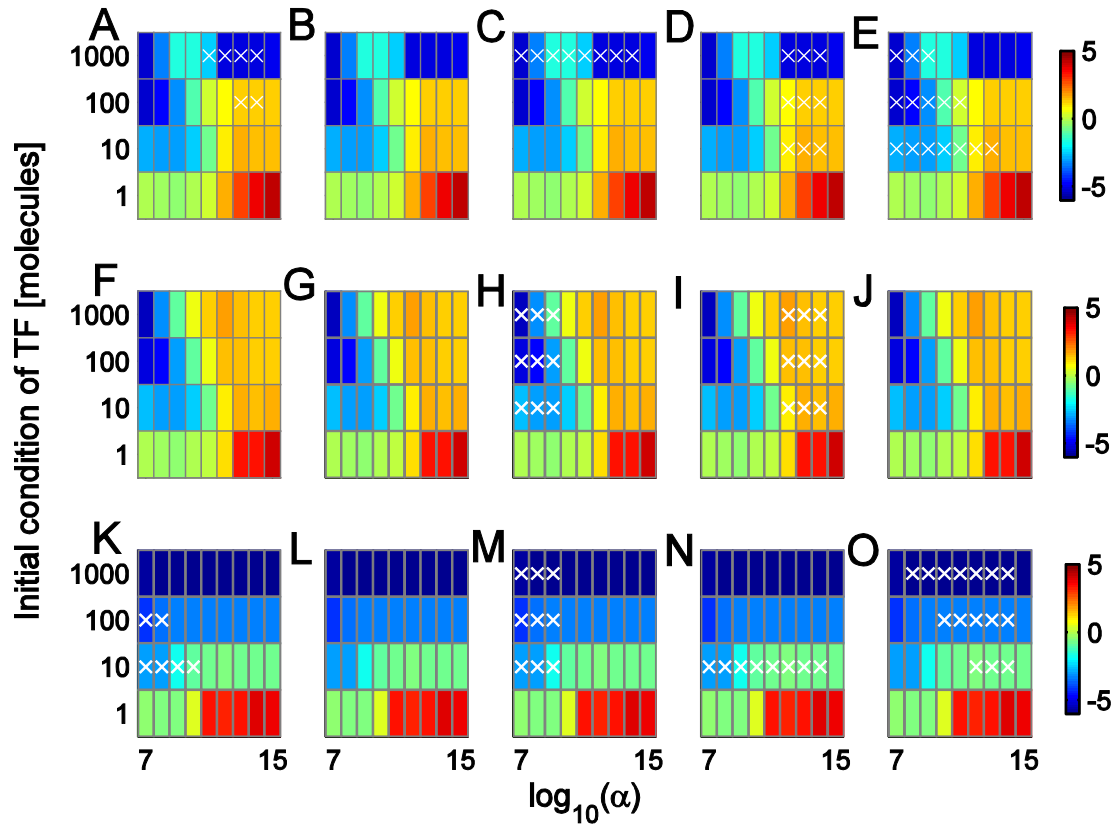


Figure S19. Feedback-dependent noise (CV) behavior of the ‘TT’ module, without assuming a QSS, as compared with previously published criteria for burst-like behavior and multimodality. Steady state protein levels were fixed by tuning the mRNA degradation rate (k_7 , A-E), the protein translation rate (k_8 , F-J), and the protein degradation rate (k_9 , K-O), respectively. Columns refer to different test criteria, namely (A,F,K) if $k_4 > k_7$ the TF distribution will follow that of mRNA (B,G,L) if $k_2+k_3 < k_7 < k_4$ the TF distribution will also follow that of mRNA (C,H,M) $k_2, k_3 < k_7$ yields bimodality (D,I,N) $k_3 < k_4$ yields bimodality and (E,J,O) if $k_7 \gg k_4$, -quantified here as an order of magnitude difference- one can observe protein bursts. Colors show $\log_{10}(\text{CV})$ and white crosses indicate cases predicted by the corresponding criterion.

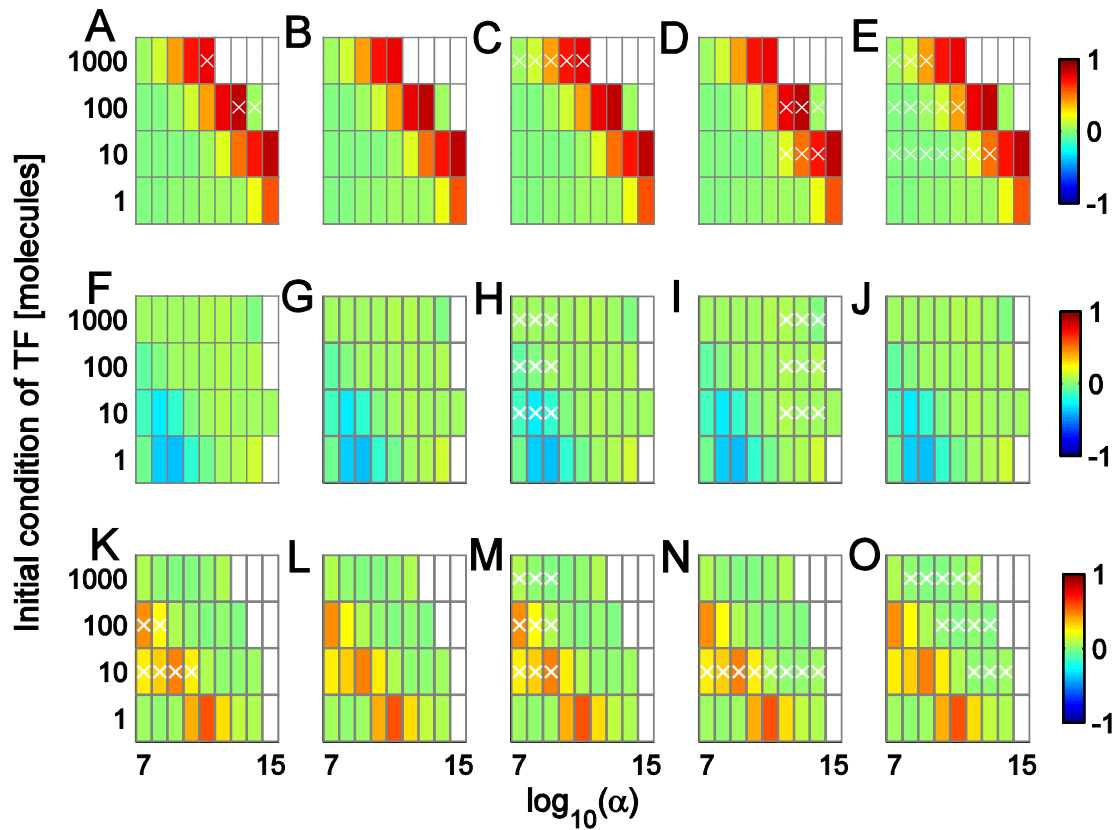


Figure S20. Time-correlation behavior of the 'TT' module, without assuming a QSS, as compared with previously published criteria for burst-like behavior and multimodality. Steady state protein levels were fixed by tuning the mRNA degradation rate (k_7 , A-E), the protein translation rate (k_8 , F-J), and the protein degradation rate (k_8 , K-O), respectively. Columns refer to different test criteria, namely (A,F,K) if $k_4 > k_7$ the TF distribution will follow that of mRNA (B,G,L) if $k_2+k_3 < k_7 < k_4$ the TF distribution will also follow that of mRNA (C,H,M) $k_2, k_3 < k_7$ yields bimodality (D,I,N) $k_3 < k_4$ yields bimodality and (E,J,O) if $k_7 \gg k_4$, quantified here as an order of magnitude difference, one can observe protein bursts. Colors show $\log_{10}(CV)$ and white crosses indicate cases predicted by the corresponding criterion. Empty boxes indicate relaxation to inactive gene state, or non-computable cases.

References

1. Stekel DJ, Jenkins DJ (2008) Strong negative self regulation of Prokaryotic transcription factors increases the intrinsic noise of protein expression. *BMC Systems Biology* 2:6
2. Slutsky M, Mirny L (2004) Kinetics of protein-DNA interaction: Facilitated target location in sequence-dependent potential. *Biophysical Journal*, 87: 4021-4035.
3. Becskei A, Serrano L (2000) Engineering stability in gene networks by autoregulation. *Nature*, 405: 590-593.
4. Elf J, Li G, Xie X.S. (2007) Probing transcription factor dynamics at the single-molecule level in a living cell. *Science* 316, 1191-1194.
5. Thattai M, van Oudenaarden A (2001) Intrinsic noise in gene regulatory networks. *Proc. Natl. Acad. Sci. USA*, 98 (15): 8614-8619.
6. McAdams HH, Arkin A (1997) Stochastic mechanisms in gene expression. *Proc. Natl. Acad. Sci. USA* 94: 814-819.
7. Hasty J, Isaacs F, Dolnik M, McMillen D, Collins J (2001) Designer gene networks: Towards fundamental cellular control. *Chaos* 11(1): 207-220.
8. Fang X, Bentley W, Zafiriou E (1995) Stochastic modelling of gene positive autoregulation networks involving signal molecules. *Biophysical Journal* 95: 3137-3145.
9. Gillespie, D. T. (1977) Exact stochastic simulation of coupled chemical reactions *J Phys Chem* **81**, 2340-2361.
10. Paulsson, J. (2005) Models of stochastic gene expression. *Physics of Life Reviews* 2, 157-175.
11. Elowitz, M. B., Levine, A. J., Siggia, E. D., Swain, P. S. (2002) Stochastic gene expression in a single cell. *Science* 297, 1183-1186.
12. Raser, J. M. & O'Shea, E. K. (2005) Noise in gene expression: origins, consequences, and control. *Science* 309, 2010-2013.
13. Hooshangi S, Weiss R (2006) The effect of negative feedback on noise propagation in transcriptional gene networks. *Chaos* **16**, 026108.
14. MacNamara S (2008) *Krylov and Finite State Projection methods for simulating stochastic biochemical kinetics via the Chemical Master Equation* (PhD Thesis, The University of Queensland).
15. MacNamara S, Bersani AM, Burrage K, Sidje RB (2008) Stochastic chemical kinetics and the total quasi-steady-state assumption: application to the stochastic simulation algorithm and chemical master equation. *J Chem Phys* **129**, 095105.
16. Munsky B, Khammash M (2006) The finite state projection algorithm for the solution of the chemical master equation. *J Chem Phys* **124**, 044104.